

Topological measures of order for imperfect two-dimensional Bravais latticesPatrick D. Shipman *Department of Mathematics and School of Advanced Materials Discovery, Colorado State University, Fort Collins, Colorado 80523, USA*

Tejas Sharath

*Department of Physics, Colorado State University, Fort Collins, Colorado 80523, USA*R. Mark Bradley *Departments of Physics and Mathematics, Colorado State University, Fort Collins, Colorado 80523, USA*

(Received 11 September 2022; accepted 20 March 2023; published 26 April 2023)

Motivated by patterns with defects in natural and laboratory systems, we develop two quantitative measures of order for imperfect Bravais lattices in the plane. A tool from topological data analysis called persistent homology combined with the sliced Wasserstein distance, a metric on point distributions, are the key components for defining these measures. The measures generalize previous measures of order using persistent homology that were applicable only to imperfect hexagonal lattices in two dimensions. We illustrate the sensitivities of these measures to the degree of perturbation of perfect hexagonal, square, and rhombic Bravais lattices. We also study imperfect hexagonal, square, and rhombic lattices produced by numerical simulations of pattern-forming partial differential equations. These numerical experiments serve to compare the measures of lattice order and reveal differences in the evolution of the patterns in various partial differential equations.

DOI: [10.1103/PhysRevE.107.044216](https://doi.org/10.1103/PhysRevE.107.044216)**I. INTRODUCTION**

Two-dimensional (2D) patterns arise in a wide variety of natural systems and laboratory experiments. Classic Rayleigh-Bénard convection experiments, for example, give rise to hexagonal or square patterns [1,2], while two-frequency parametric forcing of surface waves on a fluid can produce rhomboidal, hexagonal, and square patterns [3]. Bombarding a solid surface with a broad ion beam, on the other hand, can result in nanoscale mounds (so-called “nanodots”) arranged in hexagonal or square arrays [4–8]. These patterns are seldom perfect Bravais lattices. Defects, such as grain boundaries between regions in which the patterns have different orientations, pairs of pentagons and heptagons in otherwise hexagonal lattices, and dislocations are common.

Effective methods of characterizing the order in a 2D pattern are desirable in a number of applications. For example, hexagonal arrays of nanodots produced by ion bombardment have served as templates for the formation of arrays of nanomagnets which could potentially be used in the production of high-density magnetic data storage devices [9,10]. In such applications, one aims for as ordered a pattern as possible. A gauge of the degree of order is needed to assess the quality of the end product of fabrication methods.

A number of methods have traditionally been applied to measure the order in a 2D pattern. One such method is to compute the width of the lowest-order peak in the Fourier transform of the pattern. However, this method is difficult to apply in cases for which the peaks in the Fourier transform are not separable from the background or from each other. A second widely employed method examines how the pattern’s autocorrelation function decays with distance. If it decays exponentially, the characteristic length scale of the decay (the

correlation length ξ) gives an estimate of the range over which the order extends. However, this method does not apply if there is not a region of exponential decay in the autocorrelation function. This method has been tested in the context of imperfectly ordered hexagonal arrays of nanodots by Böttger *et al.* [11]. These authors found ξ to remain nearly constant even as order increased in their samples. Thus, ξ can be an insensitive gauge of order even in cases for which it can be measured.

A relatively new tool of computational topology called persistent homology (PH) characterizes topological features such as components or holes of various dimensions in finite point sets [12]. PH probes these features at all length scales and thus may be characterized as a geometric-topological method. PH has proved to be a powerful tool for probing topological features of data in a wide variety of applications. (See Ref. [13] for an accessible introduction to PH and its applications in materials science and Ref. [14] for a more general review.) In physics and materials science, PH methods have been applied to describe multiscale topological and geometric features of atomic configurations in silica glass [15,16], to characterize the structure of granular media and the force networks within them [17–19], and to study fluid flow [20] and crystallization mechanisms [21]. They have also been used to identify nanovoids formed during the crazing process of glassy polymers [22] and to represent energy landscapes of molecules such as n-alkanes [14].

PH has recently been applied to gauge the degree of order in imperfect hexagonal lattices [23,24]. Two measures of order were employed: the variance of H_0 [$\text{var}(H_0)$] and the H_1 sum (ΣH_1). These two measures of hexagonal order are zero for a perfect hexagonal lattice and grow larger if the lattice is

perturbed. They can be applied no matter whether the pattern is very disordered or nearly defect free. The variance of H_0 , however, cannot distinguish one type of lattice from another. The H_1 sum, on the other hand, probes hexagonal order but does not have an obvious generalization to other kinds of 2D lattice.

In this paper, we introduce PH-based measures of order that can be employed to quantify the degree of order in any imperfect 2D Bravais lattice relative to a given perfect (or *ideal*) lattice. A 2D Bravais lattice is a set $\{z_1 \vec{v}_1 + z_2 \vec{v}_2 : z_i \in \mathbb{Z}\}$ for two vectors $\vec{v}_1, \vec{v}_2 \in \mathbb{R}^2$. We will apply the introduced measures to finite subsets of such lattices (such as the set of points in a Bravais lattice that are also in a given square subset of \mathbb{R}^2) and simply refer to these as “lattices.” By an *imperfect lattice* we mean a set of points that resembles a lattice but may be a perturbation of a lattice or have defects. To make it clear when we are referring to perfect lattices, we will refer to these as *ideal lattices*. To compute the measures of order, we first choose an ideal lattice that is used as a point of reference in assessing the degree of order in imperfect 2D Bravais lattices. We then apply PH to capture topological properties of both the ideal and imperfect lattices. Briefly, PH keeps track of topological features that form (are born) or disappear (die) as a “connectivity” parameter is increased; this parameter determines how the data points are connected by edges and faces. For each topological feature, a point is added to a *birth-death* diagram whose coordinate values are the associated birth and death values of the connectivity parameter. Since the lattices consist of points in the 2D plane, PH provides two birth-death diagrams for each of the lattices—an H_0 birth-death diagram that provides information on topological components and an H_1 birth-death diagram that provides information on topological holes. We then apply a metric on point distributions to give distances between the H_0 and H_1 birth-death diagrams of the idealized and imperfect lattices. These distances, which we call WD_0 and WD_1 , respectively, are our measures of order for the imperfect lattice. To illustrate their use, we apply these measures to imperfect hexagonal, square, and rhombic patterns produced by partial differential equations. We also apply them to imperfect lattices produced by perturbing perfectly regular Bravais lattices.

This paper is organized as follows: After providing background material on persistent homology, birth-death diagrams, and a metric on point distributions called the sliced Wasserstein metric, we define our PH-based measures of order in Sec. II. We apply these measures of order to perturbations of perfect 2D lattices in Sec. III and to imperfect hexagonal, rhombic, and square lattices derived from pattern-forming partial differential equations (PDEs) in Sec. IV. The imperfect lattices derived from PDEs, and therefore the measures of order, evolve over time, and we compare this evolution for different PDEs and different choices of parameters. We conclude with a discussion of our results in Sec. V.

II. PERSISTENT HOMOLOGY, THE WASSERSTEIN DISTANCE, AND TWO MEASURES OF ORDER

Let $u(x, y, t)$ be a real-valued function of the coordinates x and y and of the time t . For the sake of specificity, we will take $u(x, y, t)$ to be the height of a surface above the

point (x, y) in the x - y plane at time t , although u could be one of many different physical quantities, including density, temperature, or electric field strength. Mounds on the surface will for brevity be referred to as “dots,” in analogy with the term “nanodot” that is often used to refer to nanoscale surface mounds. The lattice \mathcal{L} is defined to be the set of points in the x - y plane where local maxima in u are located. These lattice points are the apexes of the dots. Our goal will be to gauge the degree of order in the arrangement of lattice points.

PH is a computational tool that can be used to characterize topological features such as the number of connected components or the number of holes in a collection of data points [12]. In the present case, we will use PH to identify these features in \mathcal{L} , and so to provide us with a means to quantify the degree of order in the lattice.

In order to use PH, we create the Vietoris-Rips complex and the associated birth-death (BD) diagram from the lattice points [12]. The Vietoris-Rips complex is a simplicial complex that consists of vertices, edges, and faces and is characterized by a connectivity parameter $r \in [0, \infty)$. The BD diagram is a plot that consists of points whose horizontal and vertical coordinates specify the value of r at which some feature of the simplicial complex is created and destroyed, respectively.

Our discussion of PH will be brief and is given for the sake of completeness. Readers may find more detail and figures illustrating the construction of the Vietoris-Rips complex and the associated BD diagram in Ref. [24].

The Vietoris-Rips complex for a specific value of r is constructed in the following way. For every two points in the lattice that are a distance r or less from one another, a line is drawn between them and is included as an edge in the simplicial complex. Should three edges meet and form a triangle, the triangle is filled in and is included in the complex as a face. Vietoris-Rips complexes for a perfect rectangular lattice are shown in the first column of Fig. 1 for four values of r . The construction of the Vietoris-Rips complex for an imperfect hexagonal lattice is illustrated by Fig. 2 of Ref. [24].

To produce the BD diagram, the Vietoris-Rips complex is constructed for all values of r , starting at zero and then increasing. Two sets of points are plotted on the BD diagram, H_0 and H_1 . H_0 is the set of points that signify the creation and destruction of components in the complex, and H_1 is the set of points that signify the creation and destruction of topological holes. For $r = 0$, the complex has no edges or faces, and the total number of components is simply the number of lattice points under consideration. As r increases, edges begin to form between vertices. Each addition of an edge potentially decreases the number of components in the simplicial complex. If the number of components decreases by n at $r = \hat{r}$, then n points $(0, \hat{r})$ are added to H_0 .

As the complex is constructed, holes may develop for some values of r . These are regions where four or more edges have been joined to form a polygon but r is not yet large enough for a triangle to have formed within it. For example, suppose four lattice points are arranged in the shape of a square, and the value of r lies between the side length and the diagonal length of the square. The square encloses a hole for this value of r . When such holes are created and then closed up, points (r_b, r_d) are added to the set H_1 , where r_b is the value of r at which

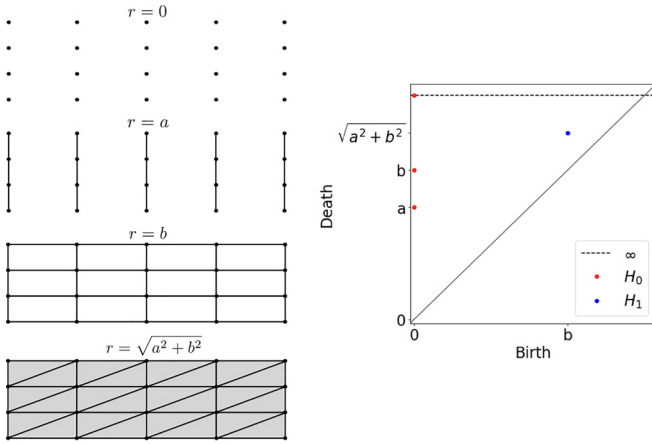


FIG. 1. Left column: Vietoris-Rips complexes built on a perfect rectangular lattice with side lengths a and b , where $b > a$. Complexes are shown at four values of the connectivity parameter r . Lines denote edges in the complexes, and faces are shown as shaded triangles. Right column: The associated BD diagram. The red points belong to H_0 and the blue points to H_1 . Note that multiple points can and do lie at the same coordinates, atop one another, and both the total number of points and ratio of the number of points at different locations depend on the size of the domain. The horizontal dashed line is located at infinity, and the dot located on it is a single point.

the hole forms and r_d is the value at which the hole closes up. For the rectangular lattice with sides lengths a and b with $a < b$, complexes are shown in the first column of Fig. 1 for $r = 0$ and the three values of r at which additional edges or faces are added. The shorter (longer) sides of the rectangles are connected at $r = a$ ($r = b$). Diagonal edges appear at $r = \sqrt{a^2 + b^2}$, thus creating triangles which are filled in by faces. Therefore, as shown in the second column of Fig. 1, rectangular lattices have points associated with H_0 at three locations in the BD diagram—one point at $(0, \infty)$, and the rest of the points are divided between $(0, a)$ and $(0, b)$. Holes form at $r = b$ and disappear at $r = \sqrt{a^2 + b^2}$, giving points with coordinates $(b, \sqrt{a^2 + b^2})$ in the H_1 BD diagram. The BD diagram for the imperfect hexagonal lattice shown in Fig. 2 of Ref. [24] is shown in Fig. 3 of that paper.

In order to quantify the degree of order in our patterns, we introduce the Wasserstein distance (WD) [25] into our analysis. The WD can be thought of as the “distance” between two distributions of points. It is the minimum distance over which points must be moved to go from one distribution to the other. The WD is also known as the “earth mover’s distance”—intuitively, one can think of the two point distributions as two different mounds of earth, and the earth mover’s distance is the minimum distance over which earth must be moved to convert one mound into the other. More explicitly, the earth mover’s distance is the sum of the distances between the points in the first distribution and their images in the second distribution under a bijection for which that sum is the minimum over all possible bijections.

One way to use the WD to produce a measure of order would be to compare the lattice points of an imperfect lattice with an ideal lattice. If the two lattices were the same, the WD would be zero, and if they were different, it would be positive.

There is a significant issue with this, however—if the “imperfect” lattice is obtained simply by rotating or translating the ideal lattice, the WD would be nonzero, even though the two lattices are essentially the same lattice and have the same degree of order. Instead of using the WD in this way, we first use PH to create BD diagrams for the idealized and imperfect lattices, and then use a variant of the WD to compare these diagrams. This allows us to make comparisons in a way that is unaffected by translations or rotations, since the BD diagram of a lattice is unchanged by these transformations.

As our first step in defining the variant of the WD distance between two BD diagrams that we will employ, we first augment each BD diagram by taking the union of the points in that diagram with the set of points on the diagonal $\mathcal{D} \equiv \{(r_b, r_d) | r_b = r_d\}$ in the birth-death coordinate plane. This provides two benefits. First, the augmented distributions have the same (uncountably infinite) cardinality, and therefore bijections may be found between them, as required to compute the Wasserstein distance. Second, points in one BD diagram that lie close to the diagonal may be mapped by a bijection to the diagonal in the second augmented BD diagram. This captures the idea that such points stem from small, “noisy” perturbations of the data and so are of limited significance [26].

Denoting the augmented BD diagrams by $\hat{H}_0 = H_0 \cup \mathcal{D}$ and $\hat{H}_1 = H_1 \cup \mathcal{D}$, our two gauges of the order in an imperfect lattice \mathcal{L} could be taken to be the WD distances between the distributions \hat{H}_0 (\hat{H}_1) for \mathcal{L} and the distributions \hat{H}_0 (\hat{H}_1) for an idealized lattice \mathcal{I} . There is a difficulty with this approach, however. In one dimension, the WD between two distributions of points has a closed form that can be approximated. The same is not true in two dimensions, however [27]. For this reason, we will employ a variant of the WD, the sliced Wasserstein distance (SWD) [28–30], rather than the WD itself. The SWD between two distributions of points S_1 and S_2 is computed by drawing an infinite number of lines of random orientation through them and making use of orthogonal projections to define corresponding one-dimensional (1D) distributions on these lines. (A detailed description of how these projections are carried out is given in the next paragraph.) The two 1D distributions on each line are then compared by computing the 1D WD, \mathcal{W} , between them. The distance \mathcal{W} between these 1D projections when averaged over a sufficiently large number of cuts is the SWD, and it gives a good approximation to the WD between the two distributions of points in two dimensions. The SWD is itself a metric [31].

The sliced Wasserstein distance between S_1 and S_2 is by definition [30]

$$SW(S_1, S_2) = \frac{1}{\pi} \int_0^\pi \mathcal{W}(S_1^\theta \cup S_{2\Delta}^\theta, S_2^\theta \cup S_{1\Delta}^\theta) d\theta, \quad (1)$$

where θ is the angle at which a line ℓ_θ is drawn as measured from the diagonal, S_i^θ is the set of points from S_i that are orthogonally projected onto the line drawn at angle θ , and $S_{i\Delta}^\theta$ is the set of points from S_i first projected onto the diagonal \mathcal{D} and then subsequently onto the line at θ , and i is 1 or 2. See Fig. 2 for an illustration of the formation of the set $S_2^\theta \cup S_{1\Delta}^\theta$. The sets $S_1^\theta \cup S_{2\Delta}^\theta$ and $S_2^\theta \cup S_{1\Delta}^\theta$ have the same cardinality even if the sets S_1 and S_2 do not. In this way, the SWD allows one

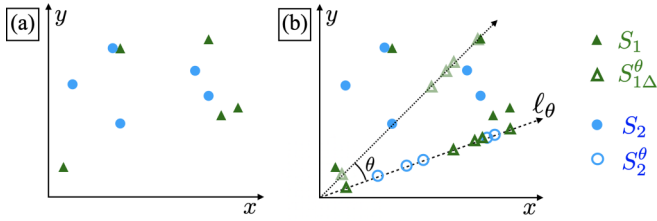


FIG. 2. Illustration of the formation of the set $S_2^\theta \cup S_{1\Delta}^\theta$ in the definition of the sliced Wasserstein distance. Two sets S_1 (filled green triangles) and S_2 (filled blue circles) in the x - y plane are shown in panel (a). In panel (b), the sets are shown together with the diagonal of the x - y plane (dotted line) and a line ℓ_θ chosen at an angle θ to the diagonal (dashed line). The set S_2^θ (open blue circles) is the orthogonal projection of S_2 onto the line ℓ_θ . The set $S_{1\Delta}^\theta$ is formed by first projecting S_1 orthogonally onto the diagonal to create $S_{1\Delta}$ (open light green triangles). The set $S_{1\Delta}^\theta$ (open green triangles) is the orthogonal projection of $S_{1\Delta}$ onto the line ℓ_θ .

to make meaningful comparisons between two point sets of different sizes. If S_1 and S_2 are BD diagrams, this implementation of the SWD also automatically satisfies the condition of first augmenting the diagrams with the points on the diagonal before computing the distance [30].

Comparing the BD diagrams obtained from \mathcal{L} with those obtained from a chosen idealized lattice \mathcal{I} yields two SWDs—one between the two H_0 BD diagrams, and another between the two H_1 BD diagrams. These distances are normalized by the number of points in their respective sets and will be called WD_0 and WD_1 , respectively. We define the degree of order of \mathcal{L} relative to \mathcal{I} to be the measures WD_0 and WD_1 . If WD_0 and WD_1 are both equal to zero, then we say that \mathcal{L} is perfectly ordered relative to \mathcal{I} . The larger the values of WD_0 and WD_1 , the less well ordered \mathcal{L} is relative to \mathcal{I} .

A limitation of the PH-based measures studied in Ref. [24] (the variance of H_0 and sum of H_1) is that they cannot be used to study an arbitrary lattice, for example, rectangular lattices. $\text{var}(H_0)$ is simply the variance of points in H_0 , excluding the point at infinity, and ΣH_1 is the sum of the vertical distances

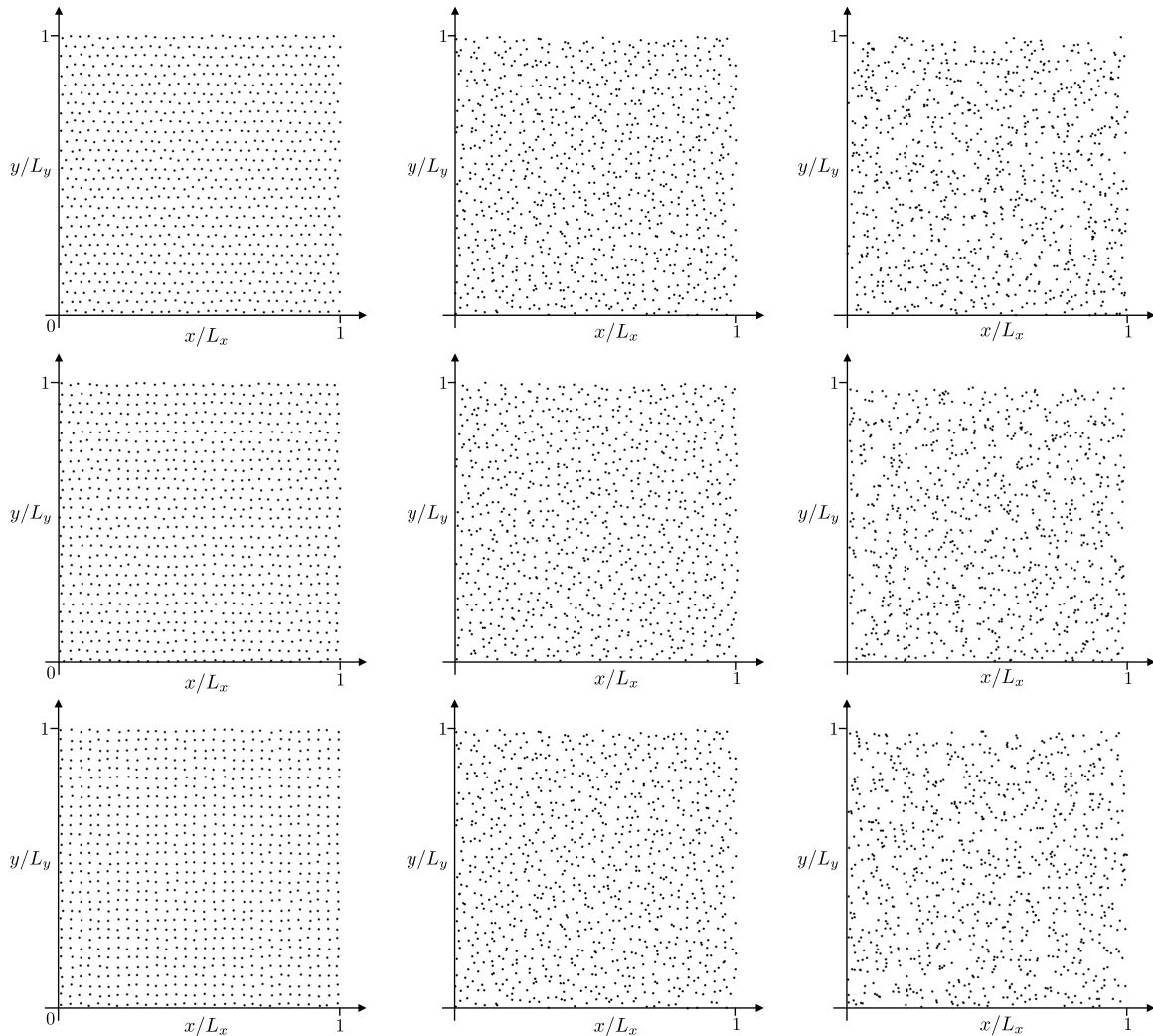


FIG. 3. Hexagonal lattices (top row), rhombic lattices with an internal angle of 75° (middle row), and square lattices (bottom row), consisting of 30×30 points and perturbed as described in the text with the parameter μ chosen to be 0.1 (first column), 0.18 (second column), and 0.3 (third column).

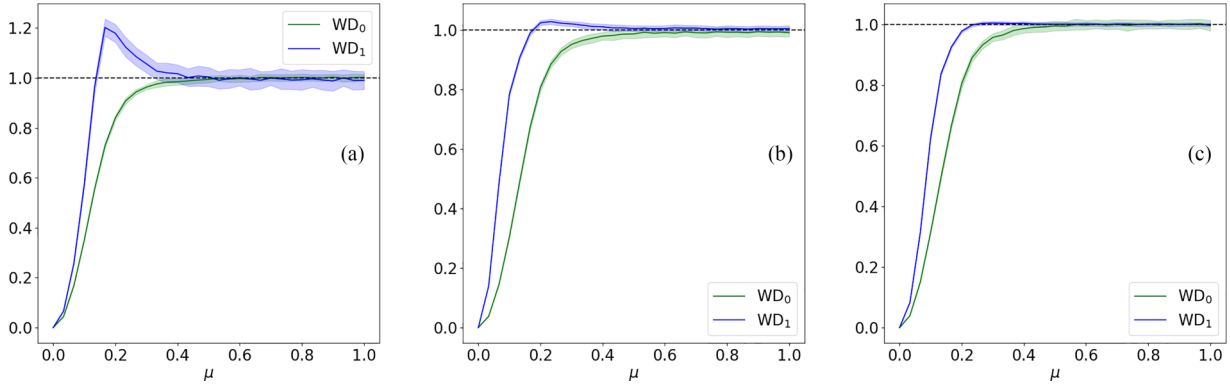


FIG. 4. The measures of order WD_0 (green) and WD_1 (blue) plotted against μ for (a) the perturbed hexagonal lattice, (b) the perturbed rhombic lattice with an internal angle of 75° , and (c) the perturbed square lattice. The variance in the measures is shown with a colored band, and each plot is averaged over 100 perturbed lattices. The lattice spacing of the ordered lattice is one in all cases.

between points in H_1 and the diagonal. Both $\text{var}(H_0)$ and ΣH_1 are zero for hexagonal lattices and are small for lattices that are close to being hexagonal. Therefore, in Ref. [24], perfect order is defined by the condition $\text{var}(H_0) = \Sigma H_1 = 0$. As shown in Fig. 1, rectangular lattices have points in H_0 at three locations in the BD diagram—one point at $(0, \infty)$, and the rest of the points are divided between $(0, a)$ and $(0, b)$, where a and b are the short and long side lengths of the rectangular unit cell. This results in $\text{var}(H_0)$ being nonzero even though the lattice is perfectly ordered. The other measure of order, ΣH_1 , is also nonzero, since all points in H_1 are located at $(b, \sqrt{a^2 + b^2})$ and this point lies above the diagonal. The SWD does not have this problem, since if the sliced Wasserstein distance between two sets of points is zero, then two sets are equal.

III. RANDOMLY PERTURBED SQUARE, HEXAGONAL, AND RHOMBIC LATTICES

To better understand the behavior of the measures of order WD_0 and WD_1 , we began by analyzing perturbed 2D lattices. We start with a perfectly ordered 2D lattice with unit lattice spacing consisting of $N \times N$ lattice points in a $L_x \times L_y$ rectangular domain. This is the ideal lattice \mathcal{I} . We compute the measures WD_0 and WD_1 of perturbations \mathcal{L} of \mathcal{I} relative to \mathcal{I} . We perturb \mathcal{I} in the following way: For each point in \mathcal{I} , we define a displacement vector \mathbf{V} with two independent components, V_x and V_y . The components are chosen randomly from a uniform distribution between 0 and $\mu^2 L_i$, where $\mu \in [0, 1]$ is a number that characterizes the size of the perturbation. Each point is then translated along its displacement vector. For $\mu = 0$, the lattice is unperturbed, and for $\mu = 1$, each point is equally likely to end up anywhere in the domain. This makes $\mu = 1$ equivalent to randomly and uniformly placing points within the domain. Periodic boundary conditions are used during the perturbation process, so that perturbed points cannot end up outside the domain. We chose to look at the case in which $N = 30$. Figure 3 shows examples of these perturbed lattices for three different values of μ .

After generating the perturbed lattices, we examined the effect that changing μ has on the measures of order. This tells us how sensitive these measures of order are at differ-

ent magnitudes of perturbation. As we shall see, for all the cases studied here, the measures of order are more effective at differentiating between two slightly different values of μ when the values are small. We analyzed hexagonal, rhombic, and square lattices in this manner. We also considered a set of points randomly chosen from a uniform distribution in the same square domain. We averaged the measures of order over 250 of these random sets and used the values to normalize our measures of order of the perturbed lattices, so that when looking at a completely random set of points, we should expect to see each of the measures of order be equal to one, on average. This allows for a fair comparison between the measures WD_0 and WD_1 .

Figure 4 shows plots of WD_0 and WD_1 vs μ for perturbed hexagonal, rhombic, and square lattices. We can use the magnitude of the derivative of a measure with respect to μ to characterize the sensitivity of these measures to changes in the level of noise. When a curve is relatively flat, the measure struggles to differentiate between differing amounts of noise, and when the curve rises or falls sharply, the measure is highly sensitive to changes in the level of noise.

The behavior of WD_0 is quite similar for all three types of lattice—the curves are monotonically increasing and are steeper at smaller μ , indicating that the measure is more sensitive in that regime than at large μ . WD_1 behaves quite differently for the hexagonal and rhombic cases than for the square lattice since the curves for the hexagonal and rhombic cases are not monotonically increasing functions of μ . WD_1 is also more sensitive for small μ than WD_0 is for all three kinds of lattice, since the slope of WD_1 is larger. For hexagonal and nearly hexagonal rhombic lattices, WD_1 alone is not sufficient to characterize the level of noise of a given lattice since it is possible for two distinct values of μ to produce disordered lattices that have the same value of WD_1 : for example, $\mu = 0.15$ and $\mu = 0.3$ give approximately the same value of WD_1 in the case of the hexagonal lattice.

IV. SIMULATIONS OF 2D PATTERN-FORMING SYSTEMS

We studied four equations of motion that produce surfaces with dots arranged in lattices with different symmetries. The four are introduced and covered in detail in the following subsections. They were selected because they produce hexagonal,

square, or rhombic lattices of dots for appropriately chosen parameter values, and because of their inherent physical interest.

We integrated the partial differential equations numerically using the fourth-order Runge-Kutta exponential time-differencing method described by Cox and Matthews [32] on the domain with $0 \leq x \leq L$ and $0 \leq y \leq L$ and employed periodic boundary conditions. An initial condition of spatial white noise with amplitude 0.001 was used. The linear terms in the partial differential equations were computed in Fourier space, and the nonlinear terms in real space. A central finite differencing scheme accurate to fourth order in the grid spacing was used to compute the nonlinear terms. In order to perform PH on the disordered arrays of dots produced by our simulations, we used the Python packages `ripser` and `persim` [33].

The process we employed to compute the measures of order WD_0 and WD_1 from surface height data is as follows: First, we located the set \mathcal{L} of local maxima on the surface by comparing each point on the surface with its nearest and next-nearest neighbors on the computational grid. For a chosen idealized lattice \mathcal{I} , we then calculated the SWDs between the H_0 BD diagrams of \mathcal{L} and \mathcal{I} to obtain WD_0 and between the H_1 BD diagrams of the two sets to obtain WD_1 .

In the case of the perturbed 2D lattices studied in Sec. III, we started with an idealized lattice and then compared it to perturbations of the lattice. In contrast, in the current case, we must judiciously choose the idealized lattice \mathcal{I} that the set \mathcal{L} of local maxima will be compared with. To select \mathcal{I} , we need to choose (1) the *type* of lattice (hexagonal, square, or rhombic), (2) the *scale* of the lattice, and (3) the *domain* of the lattice, by which we mean the finite subset of the infinite lattice that we consider. The BD diagrams of \mathcal{I} depend on all of these factors. In particular, the scale and domain of \mathcal{I} impact the number of points in \mathcal{I} and therefore the numbers of points in the BD diagrams of \mathcal{I} . Although the definition of the SWD of BD diagrams allows us to compare sets of different sizes, the WD_0 and WD_1 measures of order equal zero for two identical types of lattice only if we include the same number of points in each. We therefore arranged for \mathcal{I} to have the same number of points as \mathcal{L} . To this end, we first ran the simulation of the surface long enough that the time evolution of the surface had essentially ceased. We used this surface to choose a single ideal lattice \mathcal{I} which we employed in calculating the measures of order for the surface at any previous time in the simulation. We then noted that, for the hexagonal, square, and rhombic ideal lattices, the H_0 BD diagram includes multiple points at $(0, a)$, where a is the minimum distance between lattice points. For rhombic lattices, this last statement assumes that the internal angle θ of the rhombus is greater than $\pi/3$. This assumption will be sufficient for the examples we investigate, and so we restrict our discussion of ideal rhombic lattices to this case. Also, the H_1 BD diagram includes multiple points at (a, b) , where $b = a$ for the hexagonal lattice, $b = \sqrt{2}a$ for the square lattice, and $b = 2a \sin(\theta/2)$ for a rhombic lattice. We therefore find the BD diagrams of \mathcal{L} and determine a as the average value of the y coordinates of points in the H_0 BD diagram. If we wish to compute order relative to a rhombic lattice with internal angle larger than $\pi/3$, we determine b as the average value of the y coordinates of points in the H_1

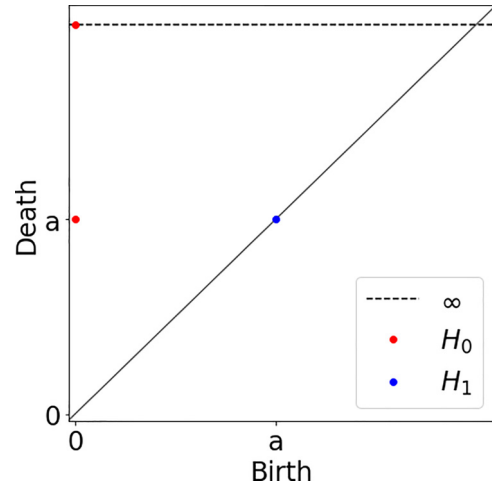


FIG. 5. The birth-death diagram of a perfect hexagonal lattice with lattice constant a . The red points belong to H_0 , and the blue points belong to H_1 . Note that multiple points lie at the same positions in the birth-death diagram, atop one another. The horizontal dashed line is located at infinity, and the dot located on it is a single point.

BD diagram. We thus determine both the type and scale of the lattice \mathcal{I} . The domain of \mathcal{I} , and therefore the numbers of points at $(0, a)$ and (a, b) in the H_0 and H_1 BD diagrams, is then chosen to be the same spatial domain as the simulation of the partial differential equation.

A. Hexagonal lattices

The first equation of motion we studied is the Swift-Hohenberg (SH) equation in two dimensions,

$$u_t = ru - (1 + \nabla^2)^2 u + gu^2 - u^3. \quad (2)$$

[We remind the reader that $u(x, y, t)$ is the height of the surface above the point (x, y) in the x - y plane at time t .]The SH equation was first introduced as a phenomenological model for analyzing transitions in behavior in Rayleigh-Bénard convection [34]. It has since been utilized widely as a model system for studies in pattern formation, including pattern selection and the formation and dynamics of defects [35,36].

In our simulations, we chose the parameters r and g so that Eq. (2) produces hexagonal arrays of dots. The BD diagram of a perfectly ordered hexagonal lattice with lattice spacing a is shown in Fig. 5. H_0 consists of multiple points at $(0, a)$ as well as a single point at infinity. H_1 , on the other hand, consists of multiple points at (a, a) . The actual number of points at each location in the BD diagram depends on the size of the lattice under consideration (i.e., the number of lattice points). The points in H_1 lie on the diagonal. This can be interpreted as holes in the simplicial complex being created and closed up at the same value of r .

Figure 6 shows a simulation of Eq. (2) for $r = 0.05$ and $g = 1$ at three different times, along with the corresponding BD diagrams. Note that the spread of points in H_0 and H_1 decreases with time, which is indicative of an increasing degree of order. This was studied in Ref. [24], where the variance of H_0 [$\text{var}(H_0)$] and the sum of vertical distances between points in H_1 and the diagonal (ΣH_1) were introduced as measures of

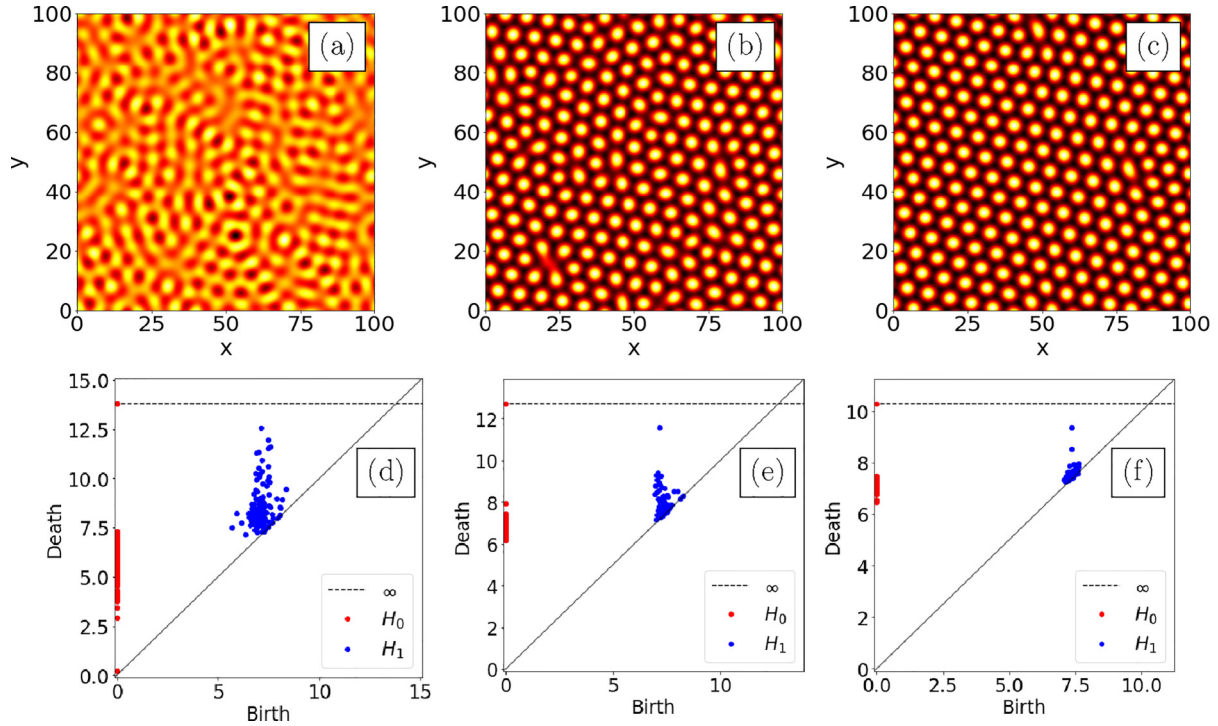


FIG. 6. Plots of simulations of Eq. (2) for the parameter values $r = 0.05$ and $g = 1$ at times (a) $t = 50$, (b) $t = 500$, and (c) $t = 5000$. Regions that are yellow (black) are high (low). The corresponding BD diagrams are shown in panels (d), (e), and (f). The domain size was 100×100 .

order for imperfect hexagonal lattices. Figure 7 shows plots of $\text{var}(H_0)$ and ΣH_1 as functions of time. Also shown are the two new measures of order, WD_0 and WD_1 as functions of time. In computing WD_0 and WD_1 as functions of time, we employed a single ideal lattice \mathcal{I} for that simulation chosen using the surface at the end time of the simulation, as described above. All four of these measures were normalized by the number of points in their respective sets, H_0 or H_1 , in the BD diagram.

The plots of ΣH_1 in Fig. 7(b) and WD_1 in Fig. 7(c) are very similar. In fact, the plots are identical, save for the different scale of the vertical axis. This is no coincidence— ΣH_1 is a scalar multiple of WD_1 for hexagonal lattices—specifically, the ratio between ΣH_1 and WD_1 is $\pi/\sqrt{2}$. This is a consequence of the definition of the SWD, along with the fact that

the idealized BD diagram for hexagons has the points in H_1 lying on the diagonal. To show this, consider a single point from the set H_1 for \mathcal{L} that lies away from the diagonal. The contribution to ΣH_1 is simply the vertical distance between this point and the diagonal, and is equal to $\sqrt{2}l$, where l is the orthogonal distance between the point and the diagonal. The contribution to WD_1 of a single point in H_1 is determined as follows: let S_1 consist of the point under consideration, and let S_2 be an arbitrary single point on the diagonal. Since S_2 is a point on the diagonal, $S_{2\Delta}^\theta = S_2^\theta$. Following Eq. (1), we have the integral

$$\text{SW} = \frac{1}{\pi} \int_0^\pi \mathcal{W}(S_1^\theta \cup S_2^\theta, S_2^\theta \cup S_{1\Delta}^\theta) d\theta. \quad (3)$$

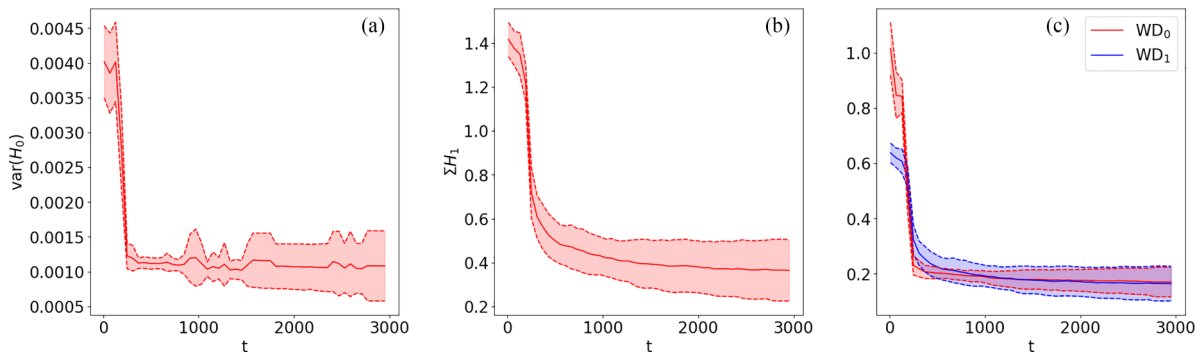


FIG. 7. Plots of the normalized measures of order vs t , averaged over 10 simulations of Eq. (2), with the shaded regions showing the variances. The parameter values in Eq. (2) were $r = 0.05$ and $g = 1$, and the domain size was 100×100 . The panels show (a) $\text{var}(H_0)$, (b) ΣH_1 , and (c) WD_0 and WD_1 .

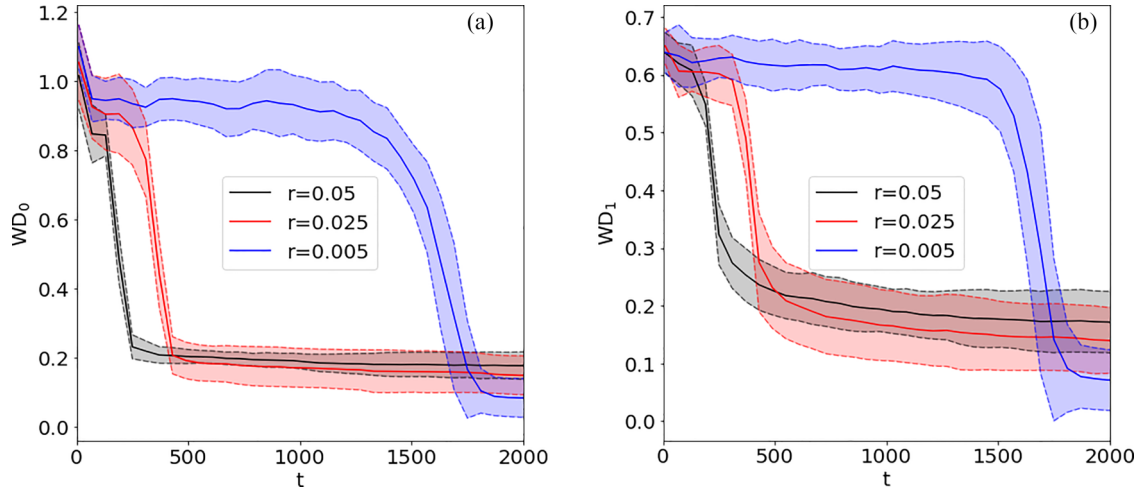


FIG. 8. Plots of (a) WD_0 and (b) WD_1 vs t for simulations of Eq. (2) for $g = 1$. In all plots the solid lines are averages and the shaded regions are the variances across 20 runs. The domain size in the simulations was 100×100 .

We can remove identical points from both sets without affecting the integrand, giving us

$$SW = \frac{1}{\pi} \int_0^\pi \mathcal{W}(S_1^\theta, S_{1\Delta}^\theta) d\theta. \quad (4)$$

Consequently, we end up computing \mathcal{W} between $S_{1\Delta}^\theta$ and S_1^θ . This quantity is simply $|l \sin \theta|$. When integrated over θ and multiplied by $1/\pi$, we find that the contribution to the SWD (i.e., WD_1) of the point under consideration is $2l/\pi$. Now consider all of the points in H_1 . If l_p is the vertical distance of a point $p \in H_1$ from the diagonal, we have $\Sigma H_1 = \sqrt{2} \Sigma_{p \in H_1} l_p$, and $WD_1 = \frac{2}{\pi} \Sigma_{p \in H_1} l_p$. The ratio between ΣH_1 and WD_1 is therefore $\pi/\sqrt{2}$. This relationship is seen only in lattices whose idealized H_1 points lie on the diagonal. For the square and rhombic lattices that are studied in the following subsections, such a relationship is not expected, nor is it present.

WD_0 is a measure that characterizes the set of bond lengths between lattice points. It is the sum of the absolute distances between points in H_0 and their mean value, and so is similar to $\text{var}(H_0)$. The more bond lengths that are different than the mean bond length, the larger WD_0 is. WD_1 , on the other hand, measures the presence of topological holes in the lattice. For a perfect hexagonal lattice, holes open and close at the same value of r and therefore holes are not persistent features of the lattice. If WD_1 is nonzero, the H_1 BD diagram has points off the diagonal, indicating persistent topological holes, and the lattice is imperfect. Lattices with a low degree of *hexagonal* order have large WD_1 values. Note that, for example, if a near-perfect square lattice were compared to an idealized hexagonal lattice, WD_0 would suggest a high degree of order is present, while WD_1 would indicate a very low degree of order. However, since the idealized H_1 set of points lies on the diagonal, WD_1 measures how hexagonal a lattice is, and so this behavior is expected. By tuning the idealized lattice, WD_0 and WD_1 are easily generalizable to square and rhombic lattices, and these cases are studied in the following subsections.

We also study the effect that changing parameter values has on the evolution of the degree of order. For the SH equation (2), we can vary the distance to threshold, r , and the

strength of the quadratic term, g . Plots of WD_0 and WD_1 are shown in Fig. 8, averaged over 20 runs for each case.

Varying the parameter g while keeping r constant did not result in significant differences for the range of g values we looked at, and so the corresponding plots are not shown here. From the plots of WD_0 and WD_1 vs t in Fig. 8, we see that as r is decreased, the transition from disorder to order occurs at a later time. However, the degree of order in the final state is also higher. This is expected behavior for this model, as r is the distance from threshold. The linear growth rate σ for a Fourier mode with 2D wave vector k for Eq. (2) is

$$\sigma(k) = r - (1 - |ck|^2)^2. \quad (5)$$

As r is decreased, the width of the band of unstable wave vectors decreases, resulting in the observed increased degree of order. Furthermore, the growth rates of all wave vectors decrease, resulting in the transition to order occurring at a later time.

We also study the damped Kuramoto-Sivashinsky equation (dKS) [37],

$$u_t = -\nabla^2 u - \nabla^4 u - \alpha u + (\nabla u)^2, \quad (6)$$

where, again, $u(x, y, t)$ is taken to be the height of the surface above the point (x, y) in the x - y plane at time t . The dKS equation has been studied as a simple model in which, as a parameter is varied, a regular, periodic pattern first develops a secondary instability and then spatiotemporal chaos occurs [37]. In the case of the dKS equation, the parameter is the damping coefficient, α . For α slightly smaller than the critical value $\alpha_c = 1/4$, the equation of motion produces a hexagonal lattice of mounds with a high degree of order. A breathing hexagonal state emerges as α is reduced through a second critical value. Finally, as α tends to zero, the equation of motion (6) behaves increasingly like the undamped Kuramoto-Sivashinsky equation, which is known to produce spatiotemporal chaos [38].

Figure 9 shows plots of the surface at $t = 5000$ for three different values of the damping coefficient α , along with the corresponding BD diagrams. Figure 10 shows the corresponding plots of WD_0 and WD_1 vs t . WD_0 and WD_1

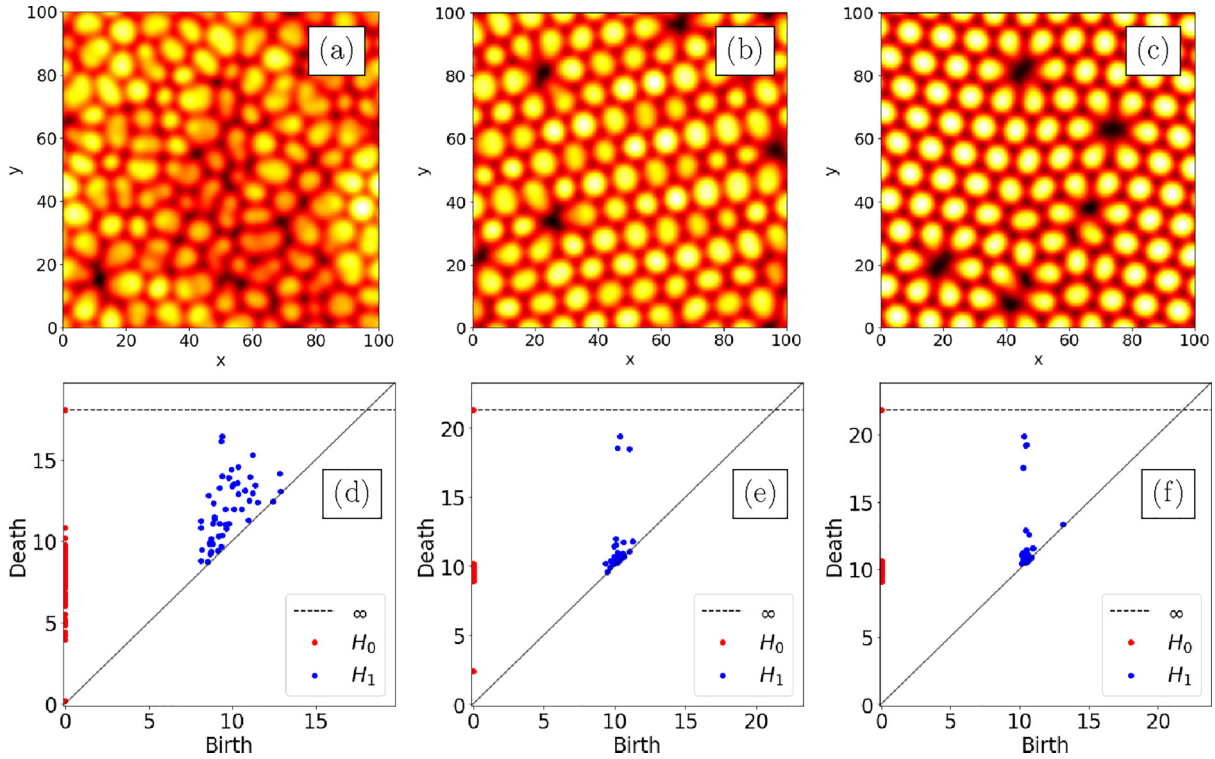


FIG. 9. Plots of simulations of Eq. (6) at $t = 5000$ for the parameter values (a) $\alpha = 0.1$, (b) $\alpha = 0.19$, and (c) $\alpha = 0.225$. The corresponding birth-death diagrams are shown in panels (d), (e), and (f). The domain size was 100×100 .

approach nearly constant values as time passes, and these values decrease with α , indicating an increase in the degree of hexagonal order as α is increased toward the critical value α_c . This makes sense considering the effect of the damping term—as α is increased, fewer Fourier modes have a positive growth rate, resulting in a narrowed band of unstable wave vectors, up until the critical value $\alpha = 0.25$ is exceeded and all Fourier modes have negative growth rates. The marked fluctuations in WD_0 and WD_1 that occur for the case $\alpha = 0$ are a consequence of the spatiotemporal chaos exhibited by the undamped Kuramoto-Sivashinsky equation.

For small values of α , the moving temporal averages of WD_0 and WD_1 are large and nearly constant; see Fig. 10(a). The measure WD_1 decreases slowly with time even for large α because there are long-lived “holes” in the pattern where dots are missing, as observed in Figs. 9(b) and 9(c). Figure 11 shows the gradual transition between these two types of be-

havior as α increases. The α dependence of the behavior is most sensitive in the range $0.10 < \alpha < 0.20$.

B. Square lattices

The third equation of motion we analyzed is the Lifshitz-Petrich (LP) equation in two dimensions [39],

$$u_t = ru - c(1 + \nabla^2)^2(q^2 + \nabla^2)^2u + \gamma u^2 - u^3. \quad (7)$$

This PDE is a generalization of the SH equation and was advanced as a model for pattern formation with two unstable length scales. It has been used to study the dynamics of surface waves on a fluid driven with two distinct frequencies [39].

The LP equation produces a variety of patterns, but we restricted ourselves to analyzing square lattices. We focused on the parameter values $c = 1$, $\gamma = 1$ and $q = \sqrt{2}$, along with

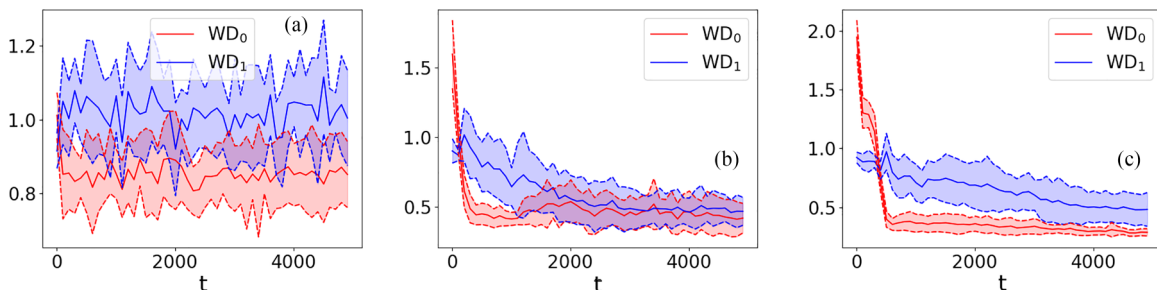


FIG. 10. Plots of WD_0 and WD_1 for simulations of Eq. (6) for the parameter values (a) $\alpha = 0.1$, (b) $\alpha = 0.19$, and (c) $\alpha = 0.225$. The domain size was 100×100 .

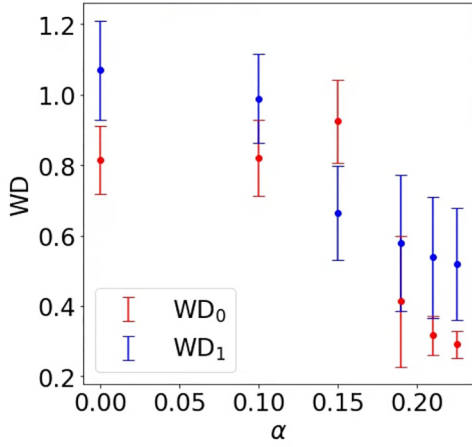


FIG. 11. Plots of WD_0 and WD_1 at $t = 5000$ vs α for simulations of Eq. (6). Data are averaged over 10 runs, and the domain size was 100×100 .

a range of r values. Equation (7) produces square lattices of dots for these parameters.

The BD diagram of an idealized square lattice with lattice spacing a is shown in Fig. 12. There are multiple points that lie at $(0, a)$ in H_0 , and multiple points lie at $(a, \sqrt{2}a)$ in H_1 . The number of such points depends on the scale of the lattice and the domain it occupies.

Figure 13 shows plots of the surface at three different times for $r = 0.015$ [Figs. 13(a)–13(c)], along with the corresponding BD diagrams [Figs. 13(d)–13(f)]. There is an initial transient that lasts up to about time $t = 550$ during which the surface remains disordered, and the surface height does not display marked maxima and minima. The surface then rapidly changes to form several regions of squares that are rotated relative to one another. This sudden transition happens for every value of r that we examined. The smaller regions occupied by square arrays of dots are quickly absorbed into larger ones, and at the end of the simulation, at $t = 2500$,

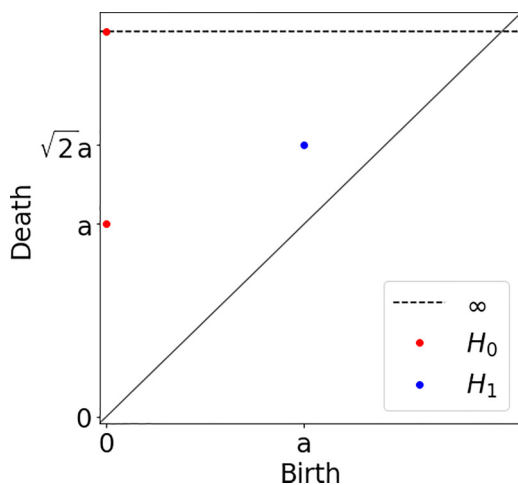


FIG. 12. The BD diagram of an idealized square lattice with lattice spacing a . Red points belong to H_0 , and blue points belong to H_1 . The horizontal dashed line is at infinity, and the dot that lies on it is a single point.

the domain typically consists of a few ordered regions. Figure 13(g) shows the evolution of the measures of order, which both drop precipitously near time $t = 550$.

In Fig. 13(c), at the end of the simulation at $t = 2500$, the surface evolution has slowed down significantly, and there exist two subdomains of different orientations. PH cannot distinguish between the two regions—two regions with the same degree of order that are rotated relative to one another produce identical birth-death diagrams, and therefore identical WD_0 and WD_1 values. However, the grain boundaries between these two regions *do* have an impact on both the BD diagrams and the measures of order. When including the grain boundaries in the PH analysis as we have done, the measures of order increase, indicating a decrease in the degree of order when compared to a subdomain in isolation. The increase in WD_0 and WD_1 is small, since the majority of the surface is in one orientation or the other, and the grain boundaries occupy a relatively small fraction of the entire domain.

For a nearly perfect surface, the full width at half maximum of the peaks in the power spectral density (PSD) can be used as a measure of the degree of order. While this does suffice for surfaces that are very nearly perfect, the presence of multiple rotated regions makes identification of the peaks in the PSD more difficult, and so the width of the peaks might not be a reliable measure of the degree of order of a surface.

Consider the two surfaces shown in Figs. 14(a) and 14(b) and the corresponding PSDs in Figs. 14(c) and 14(d). The near-perfect square array of dots shown in Fig. 14(b) has a PSD that clearly shows two primary peaks along each major axis and two secondary peaks along each diagonal. The surface shown in Fig. 14(a), on the other hand, has two distinct ordered regions in the domain that are rotated relative to one another. Within each region, however, the degree of order appears to be comparable to the near-perfect surface. In the PSD, we can see structure similar to Fig. 14(d)—two such spectra are rotated and overlaid one atop the other, corresponding to the two regions of square order in the domain.

WD_0 and WD_1 provide an excellent alternative to the Fourier transform when there are rotated regions. Since PH cannot distinguish one region from another identical but rotated region, the process of measuring the degree of order is not at all hindered by the presence of rotated regions. The interfaces between ordered regions, however, will affect the distributions of points in the BD diagrams, and the overall degree of order will be lower than a completely uniformly oriented surface, as expected.

We also studied the effect of changing the distance to threshold r for the LP equation (7). Figure 15 shows plots of WD_0 and WD_1 vs time for different values of r , averaged over 10 runs each. As r is reduced, the surface remains in a relatively flat, disordered state for a progressively longer period of time. However, after the surface suddenly transitions to a highly ordered square state, the degree of order is greater for smaller r . The linear growth rate σ for the Fourier mode with wave vector k is

$$\sigma(k) = r - c(1 - ck^2)^2(q^2 - k^2)^2. \quad (8)$$

The behavior is very similar to that of Eq. (2). As before, the growth rates of all wave vectors decrease with decreasing r , resulting in the transition to order occurring at later times.

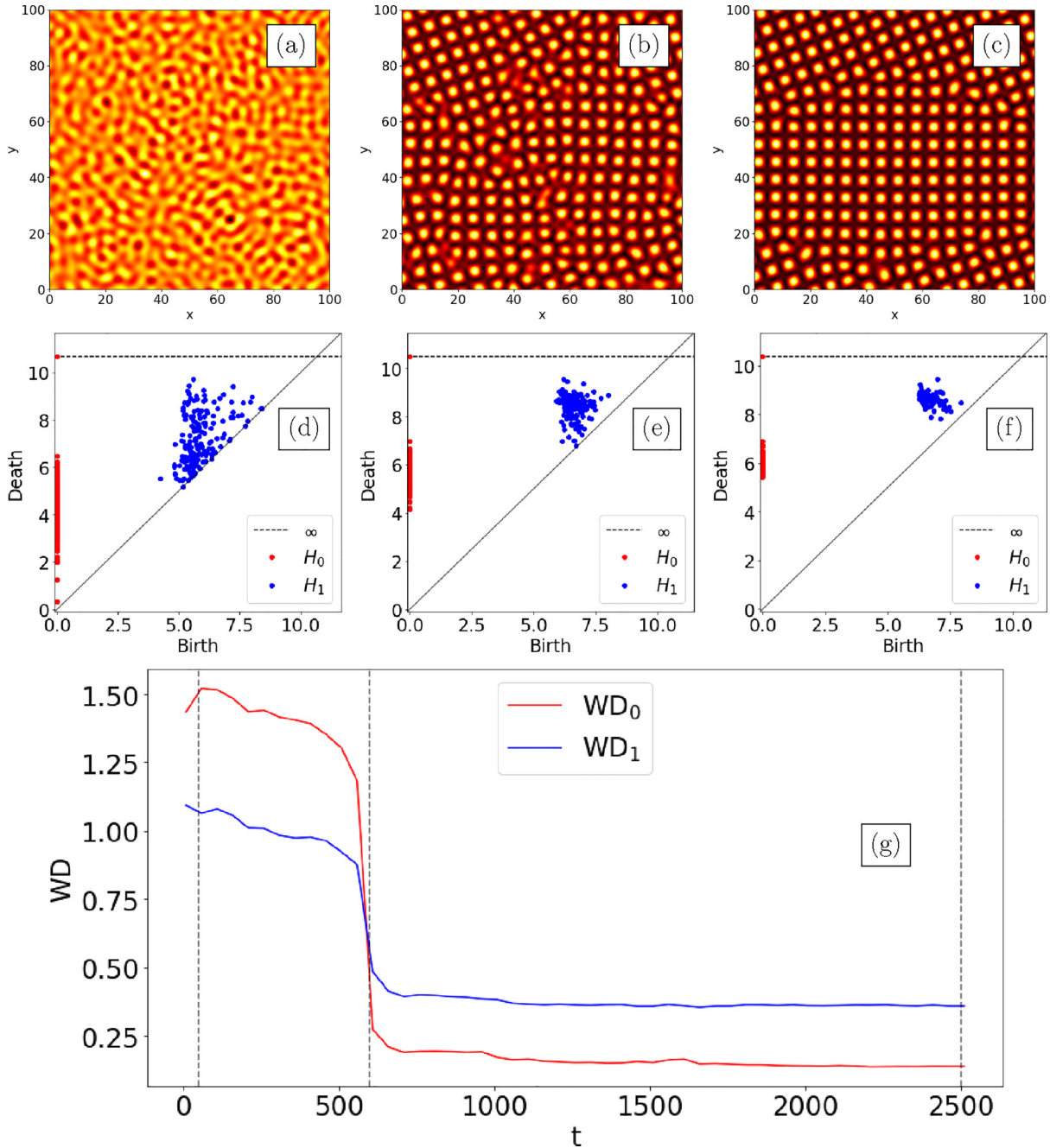


FIG. 13. Plots of simulations of Eq. (7) for the parameter values $r = 0.015$, $c = 1$, $\gamma = 1$, and $q = \sqrt{2}$ at times (a) $t = 50$, (b) $t = 600$, and (c) $t = 2500$. The corresponding BD diagrams are shown in panels (d), (e), and (f). The domain size was 100×100 . Plots of WD_0 and WD_1 are shown in panel (g). The vertical dashed lines show the times corresponding to the preceding panels.

However, as r is reduced toward the critical value $r = 0$, the widths of the bands of unstable wave vectors decrease, resulting in the observed increased degree of order at long times. This is illustrated by Fig. 16, which gives the values of WD_0 and WD_1 for five values of r at $t = 2000$ (the end time in Fig. 15), averaged over 10 runs.

An inherent timescale for the transition to order may be determined from curves such as those in Fig. 15 by first taking the derivative of WD_0 or WD_1 with respect to time. In both cases, the derivative is similar to a Gaussian function of time. The full width at half maximum of the Gaussian-like curve divided by the time at which the curve achieves its maximum

value is a nondimensional measure of how gradual the shift is, with larger values indicating a more gradual transition to order. For the curves shown in Fig. 15, these measures result in values of 0.36 ($r = 0.05$), 0.13 ($r = 0.015$), 0.085 ($r = 0.01$), and 0.054 ($r = 0.005$) for WD_0 , and 0.36 ($r = 0.05$), 0.15 ($r = 0.015$), 0.093 ($r = 0.01$), and 0.060 ($r = 0.005$) for WD_1 . Note that the transition becomes more abrupt as the critical point is approached according to both measures.

C. Rhombic lattices

Consider a perfect rhombic lattice. a is the length of the side of a rhombus in the lattice, θ is the acute interior angle of

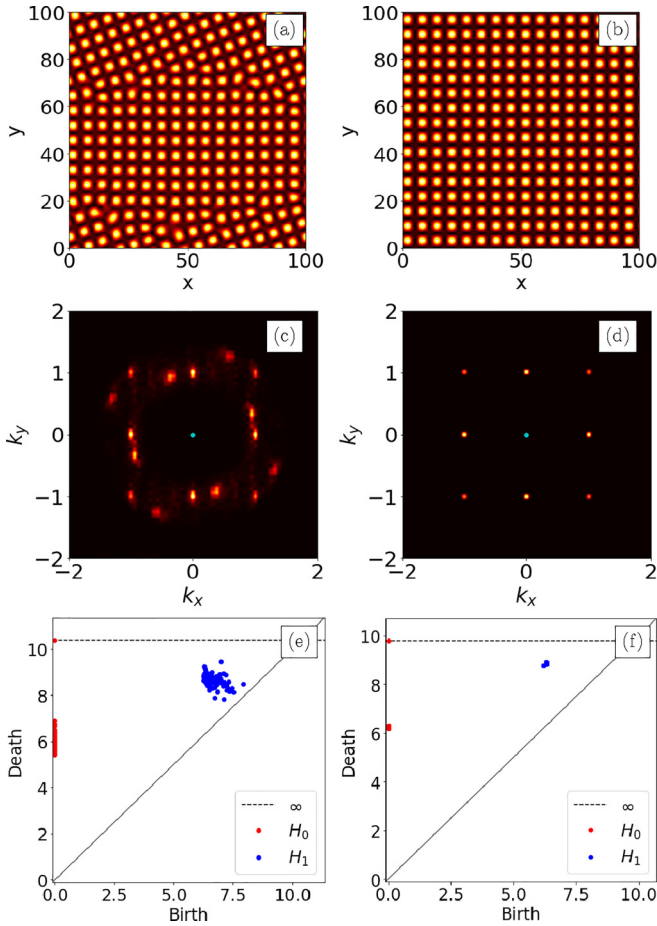


FIG. 14. Plots of the surface at $t = 2500$ from simulations of Eq. (7) for $r = 0.015$, $c = 1$, $\gamma = 1$, and $q = \sqrt{2}$. A simulation with an imperfect final state is shown in (a), and one with a nearly perfect final state is shown in (b). The corresponding Fourier spectra are shown in (c) and (d), and the corresponding BD diagrams are shown in (e) and (f).

the rhombus, and b is the length of the shorter diagonal. b is determined by a and θ , and is given by

$$b = 2a \sin(\theta/2). \quad (9)$$

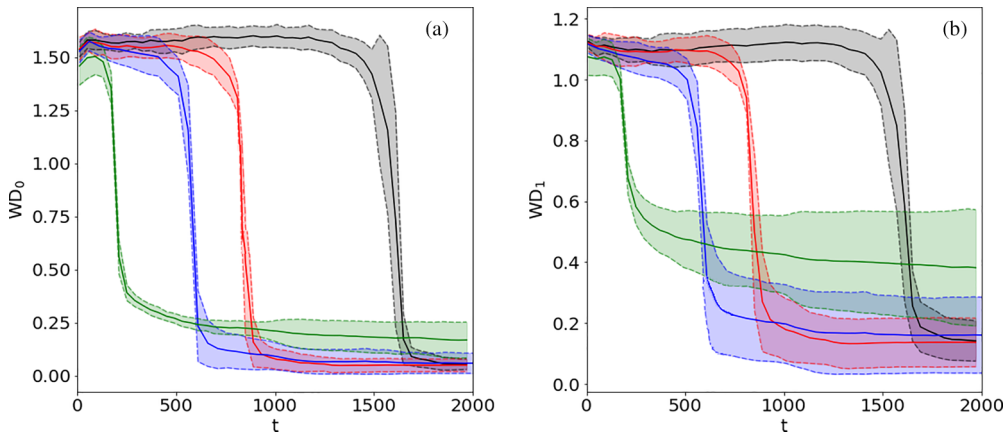


FIG. 15. Plots of (a) WD_0 and (b) WD_1 vs t for simulations of Eq. (7). The solid lines show averages and shaded regions show variances, averaged over 10 runs. The selected values of the parameter r were 0.005 (black curves), 0.01 (red curves), 0.015 (blue curves), and 0.05 (green curves). The values of the remaining parameters were $c = 1$, $\gamma = 1$, and $q = \sqrt{2}$. The domain size was 100×100 for all simulations.

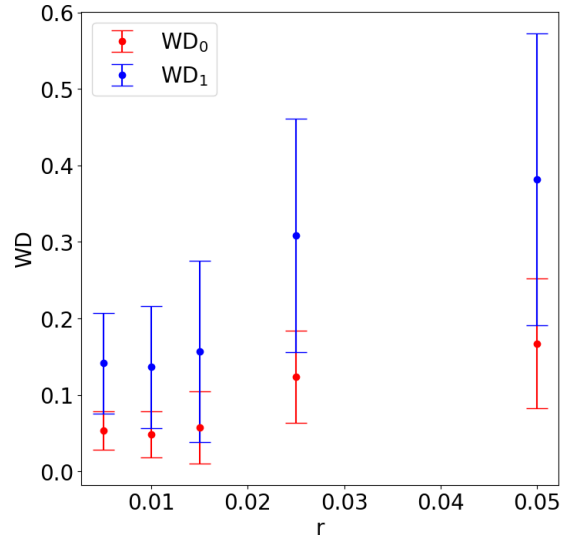


FIG. 16. Plots of WD_0 and WD_1 vs r at time $t = 2000$ averaged over 10 simulations each of Eq. (7) for the parameter values $c = 1$, $\gamma = 1$, and $q = \sqrt{2}$. The domain size was 100×100 .

Note that $\theta = \pi/2$ corresponds to a square lattice and $\theta = \pi/3$ to a hexagonal lattice. When varying θ between these bounds, b varies continuously from $\sqrt{2}a$ to a . We will restrict our attention to the case $\theta > \pi/3$, which implies that $b > a$. The BD diagram for the idealized rhombic lattice is shown in Fig. 17.

To study rhombic patterns, we simulated an equation proposed by Bestehorn to describe pattern formation in fluids [40,41], namely,

$$u_t = \epsilon u - (\nabla^2 + k_0^2)^2 u + u^3 - bu \nabla^4(u^2). \quad (10)$$

We chose the parameter values $\epsilon = 0.05$, $k_0 = 1$, and $b = 1$. Plots of the surface at three different times are shown in Figs. 18(a)–18(c) for a 100×100 domain. The associated BD diagrams, which are shown in Figs. 18(d)–18(f), reflect the increased order seen in the real-space images. Figure 19 shows plots of the measures of order WD_0 and WD_1 vs t , for two different choices of the ideal lattice, namely, a square

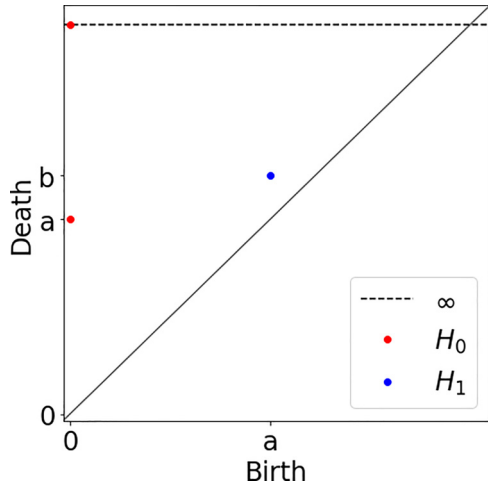


FIG. 17. BD diagram of an idealized rhombic lattice with rhombus side length a and short diagonal length b for the case $b > a$. Red points belong to H_0 , and blue points belong to H_1 . The horizontal dashed line is at infinity, and the dot that lies on it is a single point.

lattice [Fig. 19(a)] and a rhombic lattice [Fig. 19(b)]. The specific rhombic lattice chosen was different for each of 10 simulations and was determined using the average coordinates of H_0 and H_1 at $t = 2000$. The WD_0 measure (red curves in both panels of Fig. 19) is insensitive to whether a square or rhombic ideal lattice was chosen since the H_0 BD diagram for squares and rhombi both consist of multiple points at $(0, a)$. The WD_1 measure (blue curves in both panels), in contrast, is sensitive to the choice of ideal lattice; the WD_1 measure

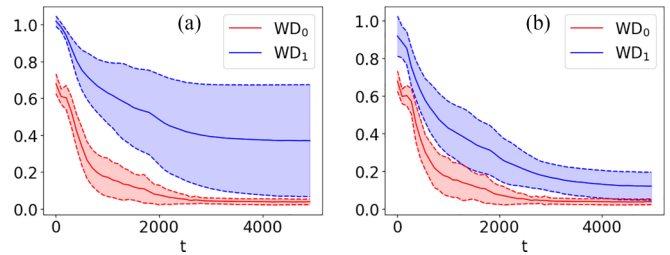


FIG. 19. Plots of WD_0 and WD_1 vs t , averaged over 10 runs of Eq. (10), with the shaded region showing the variance. The panels correspond to the WD plots for simulations on a 100×100 domain compared to (a) a square ideal lattice, and (b) rhombic ideal lattices. The parameter values in Eq. (10) were $\epsilon = 0.05$, $k_0 = 1$, and $b = 1$.

approaches zero and has smaller variance if the ideal lattice taken to be a rhombic lattice that is chosen separately for each simulation.

V. DISCUSSION

Perturbations of ideal lattices and simulations of pattern-forming partial differential equations provided the data that we analyzed in this paper. However, the algorithm for computing the WD_0 and WD_1 measures of order may be applied equally well to experimental data such as hexagonal or square arrays of nanodots that form when a solid surface is bombarded by a broad ion beam. Given an experimental surface measured by, for example, atomic force microscopy, the local maxima of that surface provide the set of points in the plane from which birth-death diagrams are computed. The next step

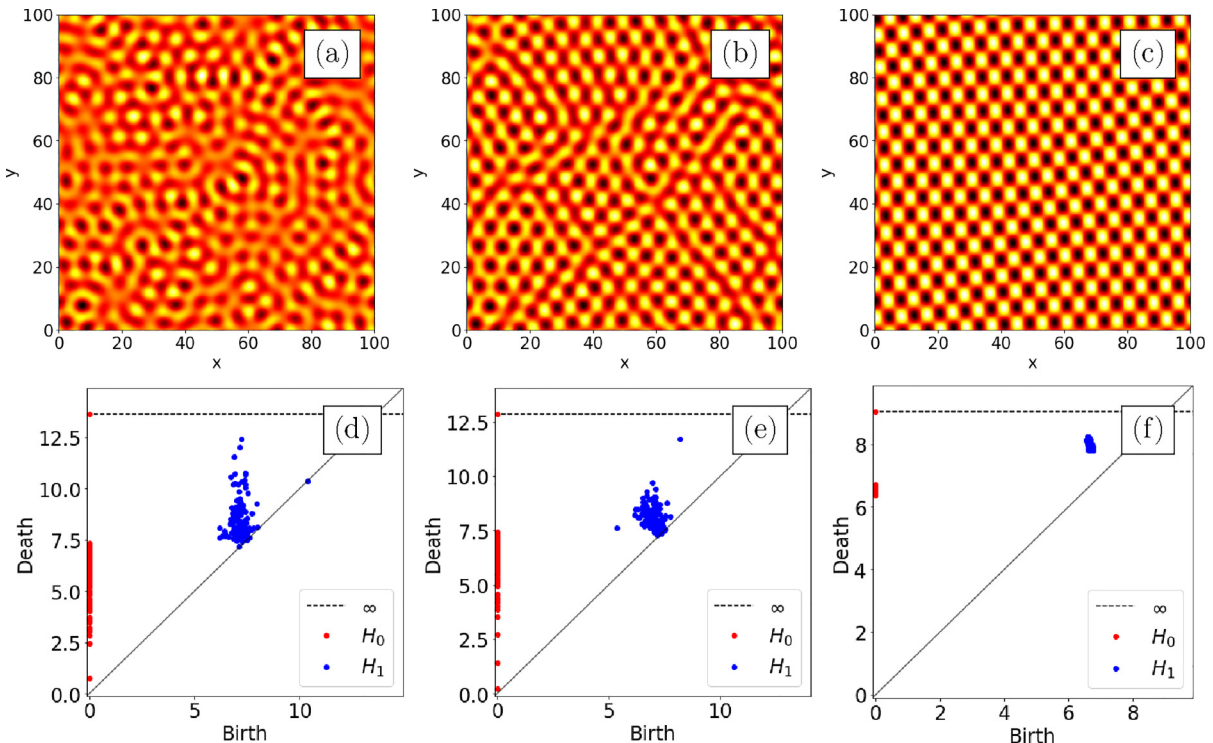


FIG. 18. Plots of simulations of Eq. (10) for the parameter values $\epsilon = 0.05$, $k_0 = 1$, and $b = 1$, at times (a) $t = 100$, (b) $t = 350$, and (c) $t = 2000$. The corresponding birth-death diagrams are shown in panels (d), (e), and (f). The domain size was 100×100 .

in computing WD_0 and WD_1 is to choose the ideal lattice that the data will be compared to. For our examples involving patterns produced by partial differential equations, we chose the ideal lattice by running the simulation long enough that the pattern was close to an ideal, periodic lattice. For experimental data, one would choose a type of lattice that most closely resembles the data and then compute the average distance between the data points to determine the length scale of the ideal lattice.

In both of the applications of the WD_0 and WD_1 measures of order we discussed, i.e., to perturbations of perfect lattices and to patterns produced by partial differential equations, we compared sets of points to a given ideal lattice. The reverse situation is also possible: one could determine, for a given set of points \mathcal{L} , the ideal lattice \mathcal{I} that yields the smallest WD_0 and WD_1 measures of order. This approach could be helpful if it is unclear which ideal lattice most closely resembles the imperfect lattice produced by an experiment.

The Wasserstein distance is a metric and therefore satisfies the reverse triangle inequality. Thus, for any imperfect lattice \mathcal{L} and ideal lattices \mathcal{I}_1 and \mathcal{I}_2 ,

$$\begin{aligned} & |\text{SW}(H_i(\mathcal{L}), H_i(\mathcal{I}_2)) - \text{SW}(H_i(\mathcal{L}), H_i(\mathcal{I}_1))| \\ & \leq \text{SW}(H_i(\mathcal{I}_1), H_i(\mathcal{I}_2)), \end{aligned} \quad (11)$$

for $i = 1, 2$. A crucial feature of persistent homology is that the birth-death diagrams H_i depend continuously on the data [12,14]. This implies that the ideal lattices \mathcal{I}_1 and \mathcal{I}_2 can be chosen to be close enough together so that $\text{SW}(H_i(\mathcal{I}_1), H_i(\mathcal{I}_2))$ is small. Equation (11) then shows that $\text{SW}(H_i(\mathcal{L}), H_i(\mathcal{I}_2))$ and $\text{SW}(H_i(\mathcal{L}), H_i(\mathcal{I}_1))$ are nearly equal. It follows that WD_0 and WD_1 change only a little if we change the ideal lattice a little. The maximum change in the measure of order given by $\text{SW}(H_i(\mathcal{I}_1), H_i(\mathcal{I}_2))$ can be easily computed due to the simplicity of the birth-death diagrams.

The WD_1 measure of order applied to perturbations of perfect 2D lattices displays a curious feature: As shown in Fig. 4, WD_1 is not a monotonic function of the perturbation parameter μ . At the local maximum, WD_1 is, in fact, larger than the average WD_1 value for a random set of points. This peak is particularly prominent for hexagonal lattices. Figures 3(a)–3(c) show perturbed hexagonal lattices for values of μ less than, equal to, and greater than the value $\mu = 0.18$ at which the maximum occurs, in an attempt to give clues to the origin of this intriguing observation, which eludes a simple explanation.

Many pattern-forming systems produce roll patterns as well as dot patterns, and transitions may occur from dot patterns to roll patterns as a parameter is varied. For example, in Rayleigh-Bénard convection experiments, transitions occur from hexagons to rolls as the Rayleigh number increases. The measures of order introduced in this paper do not handle roll patterns well; extracting local maxima from rolls typically results in strings of data points, and it is unclear which ideal lattice these strings should be compared to. Another approach to computing the birth-death diagrams may be more appropriate for roll patterns: A method called *level-set persistence* computes birth-death diagrams given surfaces rather than point sets [42]. Although we have chosen, in this paper, the more intuitive approach of analyzing the topology of point

sets, one could compute birth-death diagrams directly from surfaces produced by experiments or simulations rather than from local maxima extracted from a surface.

VI. CONCLUSIONS

Although we restricted our analysis to hexagonal, square, and rhombic lattices, the WD_0 and WD_1 measures of order introduced in this paper allow for the comparison of a set S of points in the plane to any planar Bravais lattice. Each measure outputs a single number as the measure of order of that set relative to a perfect Bravais lattice. The smaller that number, the more ordered is the set relative to the selected ideal lattice. In the method, PH is first used to find the H_0 and H_1 birth-death diagrams of both the set S and the ideal lattice. A metric on birth-death diagrams is then employed to arrive at the measure of order for S relative to the chosen ideal lattice. Making use of the sliced Wasserstein distance as the metric on distributions of points makes these measures practical since they can be computed in a reasonable amount of time.

Two measures of hexagonal order that also utilize PH were introduced in Ref. [24], namely, $\text{var}(H_0)$ and ΣH_1 . Those measures—which only be used to gauge the degree of hexagonal order in an imperfect lattice—focus on computing statistical properties of the H_0 and H_1 BD diagrams instead of employing the sliced Wasserstein distance. We showed in this paper that, for hexagonal lattices, the WD_1 measure is a scalar multiple of ΣH_1 . In this sense, WD_1 is a generalization of ΣH_1 which extends the use of PH to measure order with respect to any planar lattice.

For equations of motion that can be obtained variationally from a free energy, one may find that it is sufficient to calculate the free energy and use it as a measure of order. For models of this kind, the lower the free energy, the higher the degree of order. Of course, this method cannot be used for nonvariational equations. This further motivates our use of PH and the SWD, since our method can be applied to any model, whether or not there exists a free energy.

We studied the time evolution of the WD_0 and WD_1 measures of order for patterns produced by four partial differential equations: hexagonal patterns in the Swift-Hohenberg equation, the transition from spatiotemporally complex to hexagonal patterns in the damped Kuramoto-Sivashinsky equation, square patterns in the Lifshitz-Petrich equation, and rhombic patterns produced by the Bestehorn equation. The outputs of these differential equations are surfaces, and to calculate the degree of order relative to a Bravais lattice, we first find the positions of the local maxima of a surface. With initial conditions of spatial white noise, the patterns naturally start with a low degree of order. WD_0 and WD_1 may remain nearly constant with low degrees of order for an extended period of time before quite suddenly shifting to an ordered state. The evolution of square order in the Lifshitz-Petrich equation, Eq. (7), is a prime example of this behavior, as shown by Fig. 13. For hexagonal order, the Swift-Hohenberg equation exhibits similar behavior. Although there is only a short time before the pattern becomes well ordered in the example of Fig. 7, increasing the distance of the bifurcation parameter r from its critical value increases the time before order sets in according to these measures, as shown in Fig. 8.

In contrast to these examples in which the shift from disorder to order occurs quite suddenly and the WD measures are approximately sigmoidal functions of time, the Bestehorn equation, Eq. (10), shows a gradual shift to rhombic order that is not sigmoidal in nature; see Fig. 19(b).

The measures of order we introduced in this paper, WD_0 and WD_1 , may effectively be applied even in cases for which there is little apparent order. This is demonstrated by our study of the damped Kuramoto-Sivashinsky equation, Eq. (6). For values of damping coefficient α that are relatively close to the critical value $\alpha_c = 1/4$, relatively regular hexagonal patterns are observed, and WD_0 and WD_1 show a quick shift to order as time passes; see Fig. 10(c). In contrast, for small α , the order is weak, and WD_0 and WD_1 exhibit fluctuations of large amplitude. These fluctuations may result from spatiotemporal chaos, which is known to exist for $\alpha = 0$.

The measures of order WD_0 and WD_1 can be extended in a natural way to provide measures of order with respect to Bravais lattices in any spatial dimension, such as lattices resulting from simulations of partial differential equations in

three dimensions [43,44]. In the case of three dimensions, in addition to WD_0 and WD_1 , there would be a third measure of order WD_2 that would come from comparing the birth-death diagrams for three-dimensional holes in the imperfect and ideal lattices. It is relatively easy to gain an impression of the order in a 2D pattern simply by looking at it. This is much more difficult in three dimensions, however, and so the topological measures of order we introduced in this paper are expected to be even more useful in that context. These measures of order may also be applied to patterns occurring on spheres [45] or other nonplanar 2D surfaces whose topology prevents the formation of a perfect lattice without defects.

ACKNOWLEDGMENTS

We thank Brenden Balch for valuable discussions and two anonymous referees for valuable feedback. This work was supported by Grant No. DMS-1814941 awarded by the U.S. National Science Foundation.

-
- [1] A. V. Getling, *Rayleigh-Bénard Convection: Structures and Dynamics*, Advanced Series in Nonlinear Dynamics, Vol. 11 (World Scientific, Singapore, 1998).
- [2] P. Croquette and V. Le Galand, *Phys. Fluids* **3**, 3440 (1988).
- [3] H. Arbell and J. Fineberg, *Phys. Rev. Lett.* **84**, 654 (2000).
- [4] S. Facsko, T. Dekorsy, C. Koerdt, C. Trappe, H. Kurz, A. Vogt, and H. L. Hartnagel, *Science* **285**, 1551 (1999).
- [5] R. M. Bradley and P. D. Shipman, *Phys. Rev. Lett.* **105**, 145501 (2010).
- [6] R. M. Bradley and P. D. Shipman, *Appl. Surf. Sci.* **258**, 4161 (2012).
- [7] P. D. Shipman and R. M. Bradley, *Phys. Rev. B* **84**, 085420 (2011).
- [8] B. Ziberi, F. Frost, M. Tartz, H. Neumann, and B. Rauschenbach, *Appl. Phys. Lett.* **92**, 063102 (2008).
- [9] T. Bobek, N. Mikuszeit, J. Camarero, S. Kyrsta, L. Yang, M. A. Niño, C. Hofer, L. Gridneva, D. Arvanitis, R. Miranda *et al.*, *Adv. Mater.* **19**, 4375 (2007).
- [10] C. Teichert, J. J. de Miguel, and T. Bobek, *J. Phys.: Condens. Matter* **21**, 224025 (2009).
- [11] R. Böttger, L. Bischoff, S. Facsko, and B. Schmidt, *Europhys. Lett.* **98**, 16009 (2012).
- [12] G. Carlsson, *Bull. Am. Math. Soc.* **46**, 255 (2009).
- [13] M. Buchet, Y. Hiraoka, and I. Obayashi, in *Nanoinformatics*, edited by I. Tanaka (Springer, Singapore, 2018), pp. 75–95.
- [14] J. Mirth, Y. Zhai, J. Bush, E. G. Alvarado, H. Jordan, M. Heim, B. Krishnamoorthy, A. Pflaum, A. Clark, Y. Z, and H. Adams, *J. Chem. Phys.* **154**, 114114 (2021).
- [15] T. Nakamura, Y. Hiraoka, A. Hirata, E. G. Escolar, and Y. Nishiura, *Nanotechnology* **26**, 304001 (2015).
- [16] Y. Hiraoka, T. Nakamura, A. Hirata, E. G. Escolar, K. Matsue, and Y. Nishiura, *Proc. Natl. Acad. Sci. USA* **113**, 7035 (2016).
- [17] S. Ardanza-Trevijano, I. Zuriguel, R. Arévalo, and D. Maza, *Phys. Rev. E* **89**, 052212 (2014).
- [18] M. Kramár, A. Goulet, L. Kondic, and K. Mischaikow, *Phys. Rev. E* **87**, 042207 (2013).
- [19] M. Kramár, A. Goulet, L. Kondic, and K. Mischaikow, *Physica D* **283**, 37 (2014).
- [20] M. Kramár, R. Levanger, J. Tithof, B. Suri, M. Xu, M. Paul, M. F. Schatz, and K. Mischaikow, *Physica D* **334**, 82 (2016).
- [21] M. Saadatfar, H. Takeuchi, V. Robins, N. Francois, and Y. Hiraoka, *Nat. Commun.* **8**, 15082 (2017).
- [22] T. Ichinomiya, I. Obayashi, and Y. Hiraoka, *Phys. Rev. E* **95**, 012504 (2017).
- [23] D. A. Pearson, R. M. Bradley, F. C. Motta, and P. D. Shipman, *Phys. Rev. E* **92**, 062401 (2015).
- [24] F. C. Motta, R. Neville, P. D. Shipman, D. A. Pearson, and R. M. Bradley, *Physica D* **380–381**, 17 (2018).
- [25] C. Villani, *Optimal Transport: Old and New*, Grundlehren der mathematischen Wissenschaften, Vol. 338 (Springer, Berlin, 2009).
- [26] F. C. Motta, in *Advances in Nonlinear Geosciences*, edited by A. Tsonis (Springer, Cham, Switzerland, 2018), pp. 369–391.
- [27] S. Kolouri, K. Nadjahi, U. Simsekli, R. Badeau, and G. Rohde, in *Advances in Neural Information Processing Systems 32 (NeurIPS 2019)*, edited by H. Wallach, H. Larochelle, A. Beygelzimer, F. d’Alché-Buc, E. Fox, and R. Garnett, Vol. 32 (Curran Associates, Inc., 2019).
- [28] J. Rabin, G. Peyré, J. Delon, and M. Bernot, Scale space and variational methods in computer vision, in *Third International Conference, SSVM 2011*, edited by A. M. Bruckstein, B. M. ter Haar Romeny, A. M. Bronstein, and M. M. Bronstein (Springer, Cham, 2012), pp. 435–446.
- [29] N. Bonneel, J. Rabin, G. Peyré, and H. Pfister, *J. Math. Imaging Vision* **51**, 22 (2015).
- [30] M. Carriere, M. Cuturi, and S. Oudot, in *International Conference on Machine Learning*, edited by D. Precup and Y. W. Teh (PMLR, 2017), pp. 664–673.
- [31] N. Bonnotte, Unidimensional and evolution methods for optimal transportation, Ph.D. thesis, Université Paris Sud, 2013.

- [32] S. M. Cox and P. C. Matthews, *J. Comput. Phys.* **176**, 430 (2002).
- [33] C. Tralie, N. Saul, and R. Bar-On, *J. Open Source Softw.* **3**, 925 (2018).
- [34] J. Swift and P. C. Hohenberg, *Phys. Rev. A* **15**, 319 (1977).
- [35] T. Galla and E. Moro, *Phys. Rev. E* **67**, 035101(R) (2003).
- [36] M. Cross and H. Greenside, *Pattern Formation and Dynamics in Nonequilibrium Systems* (Cambridge University Press, Cambridge, 2009).
- [37] M. Paniconi and K. R. Elder, *Phys. Rev. E* **56**, 2713 (1997).
- [38] A. Kalogirou, E. E. Keaveny, and D. T. Papageorgiou, *Proc. R. Soc. A* **471**, 20140932 (2015).
- [39] R. Lifshitz and D. M. Petrich, *Phys. Rev. Lett.* **79**, 1261 (1997).
- [40] M. Bestehorn, in *Evolution of Dynamical Structures in Complex Systems*, edited by R. Friedrich and A. Wunderlin, Springer Proceedings in Physics, Vol. 69 (Springer, Berlin, 1992), pp. 165–196.
- [41] H. Herrero, C. Pérez-García, and M. Bestehorn, *Chaos* **4**, 15 (1994).
- [42] H. Adams and M. Moy, *Front. Artif. Intell.* **4**, 668302 (2021).
- [43] T. Callahan and E. Knobloch, *Physica D* **132**, 339 (1999).
- [44] H. Uecker and D. Wetzel, *Physica D* **406**, 132383 (2020).
- [45] P. Matthews, *Phys. Rev. E* **67**, 036206 (2003).